AFM Study of Tethered Polystyrene-*b*-poly(methyl methacrylate) and Polystyrene-*b*-poly(methyl acrylate) Brushes on Flat Silicate Substrates

Bin Zhao, William J. Brittain,* Wensheng Zhou, and Stephen Z. D. Cheng

The Department of Polymer Science, The University of Akron, Akron, Ohio 44325-3909

Received March 9, 2000; Revised Manuscript Received August 31, 2000

ABSTRACT: Atomic force microscopy (AFM) has been used to study tethered polystyrene-*b*-poly(methyl methacrylate) (PS-*b*-PMMA) and polystyrene-*b*-poly(methyl acrylate) (PS-*b*-PMA) brushes on flat substrates. The PS-*b*-PMMA surface was smooth after treatment with CH_2Cl_2; treatment with cyclohexane led to a relatively rough surface, more obvious in a brush with a thinner PMMA layer. PS-*b*-PMA brushes exhibited a different nanomorphology after treatment with CH_2Cl_2, which is may be due to the higher Flory−Huggins interaction parameter between PS and PMA. Treatment of a PS-*b*-PMMA brush with 30 nm PS and 10 nm PMMA with mixed solvents of CH_2Cl_2 and cyclohexane resulted in a variety of morphologies including a smooth surface, a rough surface, a very rough surface with irregular structures, and a very rough surface with an unusual nanomorphology. The morphological scale was dependent on the thickness of the tethered diblock brushes.

Introduction

The behavior of tethered diblock copolymer brushes is interesting because the polymer chain is covalently bonded to a solid substrate coupled with the microphase separation tendency of diblock copolymers. Theoretical studies using self-consistent-field calculations, scaling arguments, and computer simulations have indicated that tethered block copolymer brushes exhibit complex behaviors that depend on many factors.[1−8] These factors include the Flory−Huggins interaction parameter (χ), overall molecular weight (N), volume fraction of one block (f), Kuh length (flexibility of backbone), grafting density, environmental conditions (solvent, temperature), and surface free energy of each block in the air. Zhulina et al.[3] theoretically considered the phase behavior of tethered Y-shaped AB copolymer brushes in a nonselective solvent and found that lateral microsegregation occurs, and increasing χ results in an increase in the thickness of the segregated sublayer at higher grafting densities. At lower grafting densities, the brush loses its lateral homogeneity and splits into separate coils in good or Θ solvents or aggregates into "pinned micelles" or an "octopus" structure in poor solvents. Tethered linear flexible AB diblock copolymer brushes have been studied, and it was found that patterned films could be formed in a poor solvent in which the polymer−solvent interactions for each block are different.[2] Patterned films have also been predicted in selective solvents which are a Θ solvent or a marginally good solvent for one block but a poor solvent for another block.[4] In these solvents, tethered block copolymer chains self-assemble into micelles whose core is formed by less soluble block; the more soluble blocks form a shell around the core. An ordered array of these micelles results in a patterned film.

We have synthesized tethered polystyrene-*b*-poly(methyl methacrylate) (PS-*b*-PMMA) brushes and polystyrene-*b*-poly(methyl acrylate) (PS-*b*-PMA) brushes by sequential carbocationic polymerization and atom transfer radical polymerization from initiator-terminated SAMs.[9−11] We reported a nanopattern formation from tethered PS-*b*-PMMA brushes in a previous publication.[12] In this paper, we detail an AFM study of the response of tethered PS-*b*-PMMA and PS-*b*-PMA brushes to different solvent treatments. AFM is a good technique to study the surface morphology of polymer materials[13−15] and has been used extensively in investigating polymer brushes.[16−19] In particular, tapping mode AFM is especially suitable to polymer brushes studies. It offers the ability to perform high-resolution profiling of surface morphology and nanostructure (a few nanometers lateral and subnanometer vertical in imaging of nonperiodic topographic features) and the study of local material properties. Also, height images recorded in a light tapping mode accurately reproduce the true topography of soft samples. In this study, tapping mode AFM has been used to study the surface morphology of tethered diblock copolymer brushes.

Experimental Section

Materials. PS-*b*-PMMA and PS-*b*-PMA brushes were synthesized by sequential carbocationic polymerization and atom transfer radical polymerization, which has been detailed in other publications.[9−11] Cyclohexane (Aldrich, anhydrous) and CH_2Cl_2 (Fisher Scientific) were used as received.

Characterization Methods. Contact angles were determined using a Rame Hart NRL-100 contact angle goniometer equipped with an environmental chamber and tilting base mounted on a vibrationless table (Newport Corp.). Advancing and receding values were determined using the tilting stage method. Drop volumes were 10 μL. Ellipsometric measurements were performed on a Gaertner model L116C ellipsometer with He−Ne laser (λ = 632.8 nm) and a fixed angle of incidence of 70°. For the calculation of the layer thickness, a refractive index of n = 1.500 was used for the polymer films. X-ray photoelectron spectroscopy (XPS) was performed on a Perkin-Elmer instrument using Al Kα radiation at The MATNET Surface Analysis Center at Case Western Reserve University. The incidence angle of X-rays was 45° with respect to surface normal. Survey spectra were taken after the sample was treated with different solvents. AFM was performed using a Multimode scanning probe microscope (Digital Instruments) in tapping mode with a silicon tip. The AFM images were obtained at room temperature in air.

Treatment of Tethered PS-*b*-PMMA and PS-*b*-PMA Brushes with CH_2Cl_2. The PS-*b*-PMMA or PS-*b*-PMA brushes were immersed in 20 mL of CH_2Cl_2 for 30−45 min at room temperature. The samples were removed from the solvent and

10.1021/ma000434e CCC: $19.00
Published on Web 10/25/2000

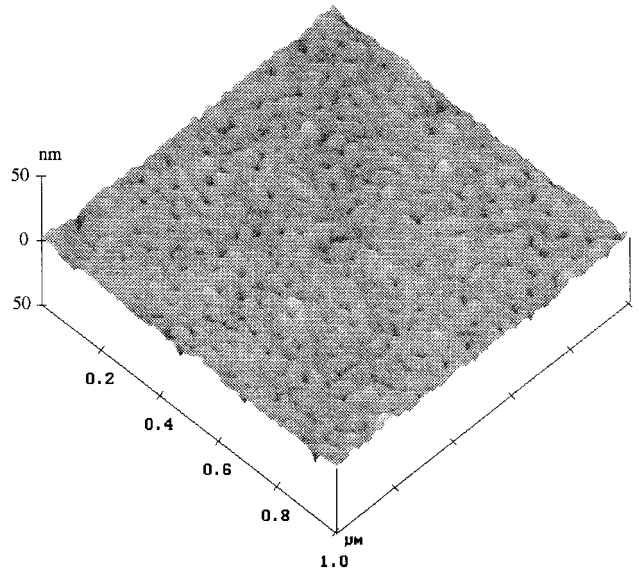

Figure 1. AFM image of a PS-*b*-PMMA brush with 23 nm PS and 14 nm PMMA after treatment with cyclohexane at 35 °C for 45 min.

dried with a stream of clean air followed by characterization with tensiometry, XPS, and AFM.

Treatment of Tethered PS-*b*-PMMA and PS-*b*-PMA Brushes with Cyclohexane. The PS-*b*-PMMA or PS-*b*-PMA brushes were immersed in cyclohexane and heated to 35 °C for 30−60 min. The sample was then removed from the solvent and dried with a stream of clean air. Tensiometry, XPS, and AFM were used to characterize the brushes.

Treatment of PS-*b*-PMMA Brushes with Mixed Solvents of CH_2Cl_2 and Cyclohexane. A PS-*b*-PMMA brush with a 30 nm thick PS layer and a 10 nm thick PMMA layer was used in this series of experiments. The sample was first immersed in CH_2Cl_2 for 30 min to recover the original state before it was treated with mixed solvents of CH_2Cl_2 and cyclohexane of different volume ratios at 35 °C for 30 min. After each treatment, the sample was characterized by tensiometry and AFM. CH_2Cl_2 and cyclohexane mixtures with volume ratios of 8:2, 6:4, 5:5, 4:6, and 2:8 were used to treat the sample.

Gradual Treatment of Tethered PS-*b*-PMMA Brushes with Mixed Solvents of CH_2Cl_2 and Cyclohexane. The PS-*b*-PMMA brushes and PS brushes were immersed in CH_2Cl_2 at 35 °C for 30 min. Fifty percent of the solvent was replaced with an equal volume of cyclohexane. The sample was treated in the resulting mixed solvent for 30 min at 35 °C. This procedure was repeated until cyclohexane: CH_2Cl_2 > 99.5:0.5 (v/v). After the sample was removed from the solvent and dried by a clean air stream, it was studied by tensiometry, XPS, and AFM.

Results and Discussion

Tethered PS-*b*-PMMA Brushes. For a tethered PS-*b*-PMMA brush with 23 nm PS and 14 nm PMMA, the tapping mode AFM image of a 1 μm × 1 μm area after treatment with CH_2Cl_2 revealed a smooth, featureless surface. If one uses a concept of roughness, which is defined as root-mean-square of height deviations taken from the mean data plane, the roughness of this film surface is 0.8 nm. The advancing and receding water contact angles of this surface are 74° and 59°, which are the same as those of a PMMA film prepared by spin-casting.

Figure 1 shows the surface morphology of this sample after treatment in cyclohexane at 35 °C for 45 min. The advancing water contact angle for this surface was 99°. Previous studies demonstrated that the topmost layer

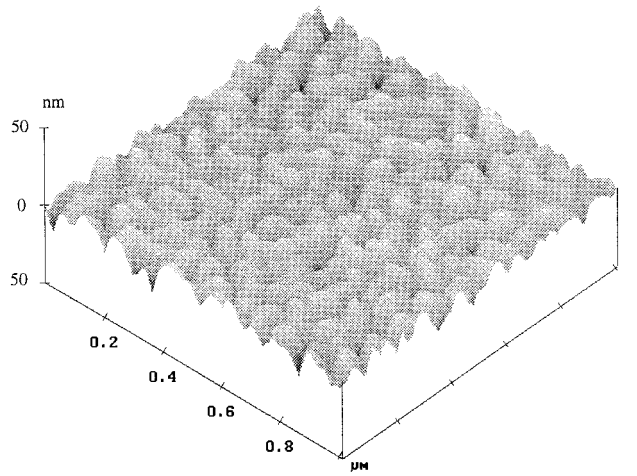

Figure 2. AFM image of a PS-*b*-PMMA brush with 29 nm PS and 3 nm PMMA after treatment with cyclohexane at 35 °C for 45 min.

is composed of PS blocks.[11] An irregular wormlike network structure appeared on the film surface with a roughness of 1.8 nm. We speculate that the PS blocks were swollen by cyclohexane while the PMMA blocks migrated to avoid contact with cyclohexane. Both effects lead to opposite movement of the two blocks, and hence networks formed. Many holes with various depths (up to 11 nm) were generated.

The mobility of tethered PS-*b*-PMMA chains in cyclohexane is low. For diblock copolymer brushes with a relatively thin PMMA layer, we believe that it is easier for tethered block copolymer chains to reorganize themselves and localize PS blocks at the interface. Figure 2 shows the AFM image of a PS-*b*-PMMA brush with 29 nm PS and 3 nm PMMA after treatment with cyclohexane at 35 °C for 45 min. The irregular wormlike structure is more obvious, and the surface roughness is 4.2 nm. The typical feature size is around 55 nm, and the height difference is as high as 14 nm. After treatment with CH_2Cl_2 at room temperature for 45 min, the AFM image of this sample reveals a featureless surface with a roughness is 0.8 nm, and the samples exhibited advancing and receding water contact angles of 75° and 60°.

AFM of Tethered PS-*b*-PMA Brushes. Tapping mode AFM of tethered PS-*b*-PMA brushes revealed a different morphology after treatment with CH_2Cl_2 compared to PS-*b*-PMMA brushes. Figure 3 shows the AFM image of a tethered PS-*b*-PMA with 24 nm PS and 9 nm PMA after treatment with CH_2Cl_2. An interconnected network with numerous isolated pits appeared on the surface of this sample; the surface roughness is 2.4 nm. The AFM image is similar to the morphology of spinodal phase separation in polymer blends. The average pit depth is 9 nm, and the average width of the network is around 50 nm. Water advancing and receding contact angles of this surface are 68° and 55°.

We expected that the surface features of PS-*b*-PMA brushes would be similar to PS-*b*-PMMA, but the result is very different. An important parameter in determining phase morphology in bulk diblock copolymers is the Flory−Huggins interaction parameter, χ. To better understand our results, we calculated the interaction parameters of PS and PMA vs PS and PMMA. Using the quadratic function $\chi = A + B/T + C/T^2$, the interaction parameter of PS and PMMA in a blend can be calculated from the following equation, $\chi_{PS-PMMA} =$

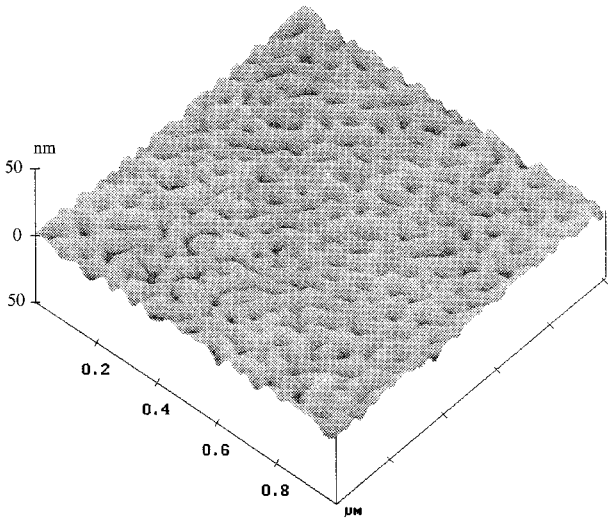

Figure 3. AFM image of a PS-*b*-PMA brush with 24 nm PS and 9 nm PMA after treatment with CH_2Cl_2 at room temperature for 45 min.

$0.0129 + 1.96/T$. The Flory−Huggins interaction parameter can be estimated from differences in solubility parameters of the pure components, δ_I, which in turn are related to their cohesive energy densities. The relationship is expressed by the following equation:

$$\chi_{AB} = V_r(\delta_A - \delta_B)^2/RT$$

V_r is the reference (molar) volume. The solubility parameters can be obtained from the literature.[20] The values for the PS, PMMA, and PMA solubility parameters are

$$\delta_{ps} = 18.72 \text{ MPa}^{1/2} \quad T = 35 \text{ °C}$$

$$\delta_{PMMA} = 18.58 \text{ MPa}^{1/2} \quad T = 35 \text{ °C}$$

$$\delta_{PMA} = 20.77 \text{ MPa}^{1/2} \quad T = 35 \text{ °C}$$

We assumed that the V_r is a constant for the estimation of $\chi_{PS-PMMA}$ and χ_{PS-PMA}:

$$\chi_{PS-PMA}/\chi_{PS-PMMA} = (\delta_{PS} - \delta_{PMA})^2/(\delta_{PS} - \delta_{PMMA})^2$$
$$= (18.72 - 20.77)^2/$$
$$(18.72 - 18.56)^2 = 164$$

Estimation from the solubility parameters of these systems indicated that the Flory−Huggins interaction parameter of PS and PMA is 164 times larger than that of PS and PMMA. This may be one reason for the formation of different morphologies in PS-*b*-PMA vs PS-*b*-PMMA brushes. We speculate that the strong segregation between PS and PMA results in phase separation not only in vertical direction but also in lateral direction, which is illustrated in Scheme 1. The AFM image of a PS-*b*-PMA brush with 25 nm PS and 6 nm PMA after treatment with CH_2Cl_2 is similar to the AFM image in Figure 3 except the domains did not form an interconnected network. We speculate that the amount of PMA is insufficient for formation of an interconnected network with a thinner PMA layer.

Treatment of a PS-*b*-PMA brush with 24 nm PS and 9 nm PMA with cyclohexane at 35 °C for 60 min resulted in a hemispherical domain morphology, which is shown in Figure 4. The average domain size is around 55 nm, and the surface roughness is 2.8 nm. The water advancing contact angle is 99°. For a PS-*b*-PMA brush with 27 nm PS and 1.5 nm PMA, the advancing and receding contact angles are 74°and 59° after treatment with CH_2Cl_2. It is surprising to find that the contact angles of PMA film prepared by spin-casting are 83° and 64°. This issue will be discussed later.

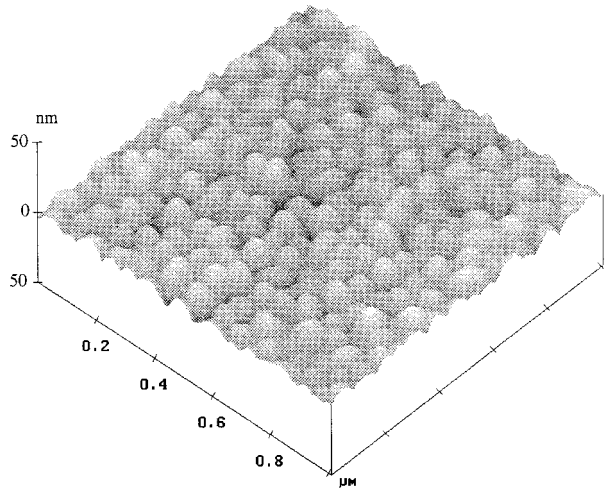

Figure 4. AFM image of a PS-*b*-PMA brush with 24 nm PS and 9 nm PMA after treatment with cyclohexane at 35 °C for 1 h.

Scheme 1. Speculative Models for PS-*b*-PMMA and PS-*b*-PMA Brush Structure after Treatment with CH_2Cl_2

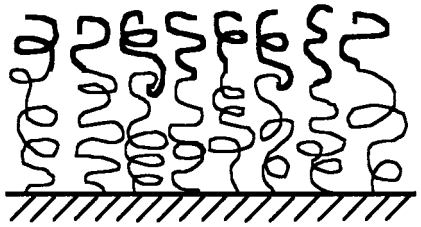

PS-*b*-PMMA brush after treatment with CH_2Cl_2

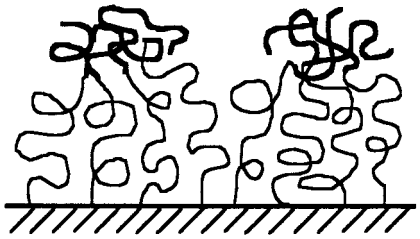

PS-*b*-PMA brush after treatment with CH_2Cl_2

AFM of Tethered PS-*b*-PMMA after Treatment with Mixed Solvents. The mobility of polymer chains in tethered diblock copolymer brushes in cyclohexane is highly restricted due to the covalent bond to the silicate surface. To increase the mobility of the tethered polymer chains, samples were treated with a series of mixed solvents of CH_2Cl_2 and cyclohexane with different volume ratios at 35 °C for 30 min followed by AFM analysis (Figure 5a−f′; water advancing contact angles are shown in Figure 5). The sample was first immersed in CH_2Cl_2 for 30 min to recover the original state before it was treated with different solvent ratios. This original state refers to one that has PMMA chains at the air interface with an advancing contact angle of 74° and a low surface roughness. A PS-*b*-PMMA brush with 30 nm PS and 10 nm PMMA was used in this study. Figure

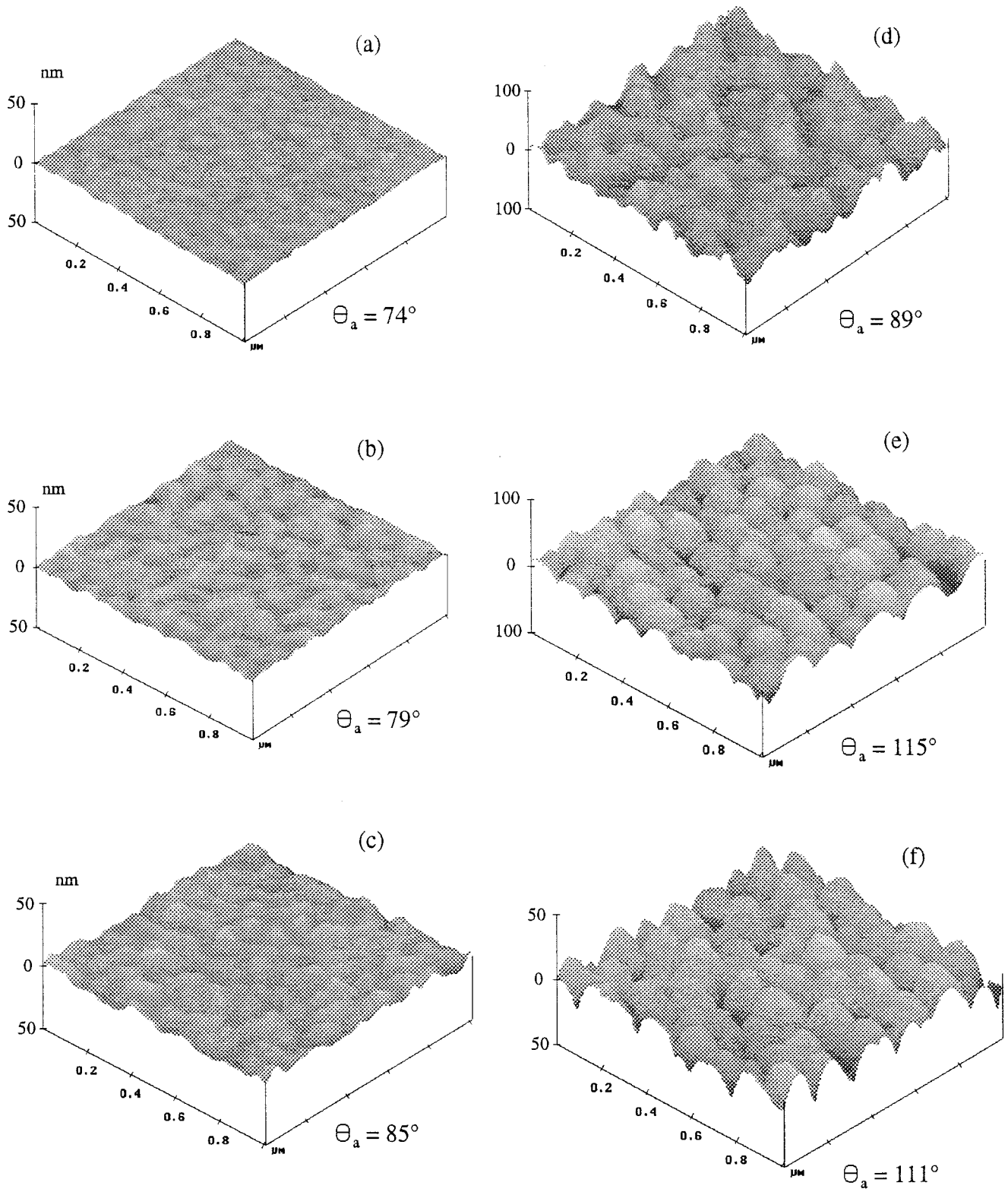

Figure 5. AFM images of a PS-*b*-PMMA brush with 30 nm PS and 10 nm PMMA after treatment with a series of mixed solvents of CH_2Cl_2 and cyclohexane with different volume ratios at 35 °C for 30 min. CH_2Cl_2/cyclohexane (v/v) = 10:0 (a), 8:2 (b), 4:6 (c), 5:5 (d), 4:6 (e), and 2:8 (f); water advancing contact angles (θ_a) are listed with each figure.

5a shows the AFM image of this sample after treatment with 100% CH_2Cl_2. The featureless surface is smooth with a roughness of 0.7 nm. Treatment with a mixed solvent of CH_2Cl_2 and cyclohexane with a volume ratio of 8:2 increased the surface roughness to 1.3 nm (Figure 5b). The sample was then reimmersed in CH_2Cl_2 at room temperature for 30 min to recover its original state followed by treatment with 6:4 (v/v) CH_2Cl_2 : cyclohexane at room temperature for 30 min. The roughness increased to 2.6 nm (Figure 5c). Figure 5d shows the AFM image of this sample after treatment with 5:5 (v/v) CH_2Cl_2:cyclohexane; the surface roughness was 11.6 nm with the appearance of many irregular domains.

The most interesting AFM images of this sample were obtained after the sample was treated with 4:6 and 2:8 (v/v) CH_2Cl_2:cyclohexane. The AFM images are shown

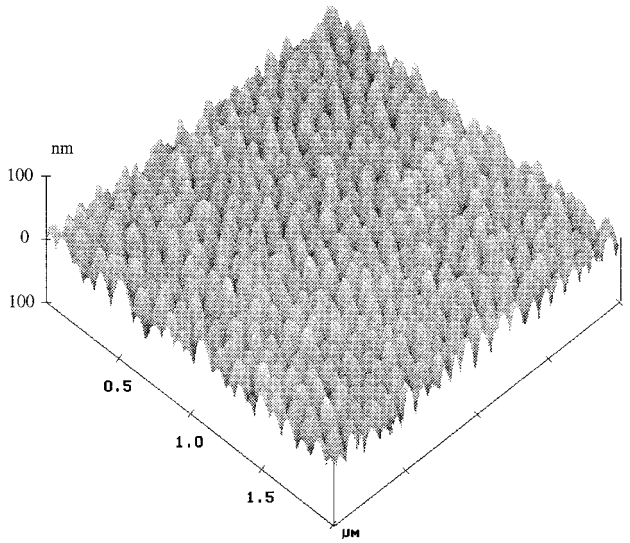

Figure 6. Nanomorphology formed from a PS-*b*-PMMA brush with 23 nm PS and 14 nm PMMA under the conditions described in the text.

in Figure 5e,f. In Figure 5e, the surface consisted of seemingly regular, round domains with a roughness of 8.9 nm. The advancing and receding contact angles were 115° and 92°, which are higher than the characteristic values of PS. Obviously, surface roughness makes a contribution to the values of contact angles. This issue will be discussed in detail later. In Figure 5f, a similar structure appears on the surface of this PS-*b*-PMMA brush with a surface roughness of 7.7 nm.

With increasing cyclohexane content, which favors PS more than PMMA, the surface became rougher. These experiments demonstrated that the tethered PS-*b*-PMMA diblock copolymer brushes can form a variety of morphologies that include a smooth surface, a rough surface, a very rough surface with irregular structures, and a very rough surface with unusual nanomorphologies depending on the volume ratio of CH_2Cl_2 to cyclohexane. We believe that it is important that the tethered polymer chains have sufficient mobility to reorganize themselves in order to achieve these nanomorphological structures.

To further increase the mobility of the tethered diblock copolymer chains and provide more opportunity to the tethered polymer chains to reorganize themselves, another experiment was carried out. A PS-*b*-PMMA brush with 23 nm PS and 14 nm PMMA was immersed in CH_2Cl_2 at 35 °C for 30 min followed by replacement of 50% of the solvent with equal volume of cyclohexane. The purpose of this experiment was to gradually change the solvent composition rather than abrupt changes like the study just discussed. The sample was treated in the resulting mixed solvent for 30 min at 35 °C. This procedure was repeated until cyclohexane:CH_2Cl_2 (or $CHCl_3$) > 99.5:0.5 (v/v). The sample was then removed from the solvent and dried with a stream of clean air and subjected to AFM study. The final AFM image is shown in Figure 6. A nanopattern was obtained from this tethered diblock copolymer brush after the treatment described above. This nanomorphology consisted of an seemingly periodic array with an average domain diameter of 85 nm. The height of the typical domain was 55 nm although the original thickness of this sample was only 37 nm. The advancing contact angle of this film was 120°, which is 21° higher than the characteristic value of PS. The surface roughness was 13.1 nm. We speculate that with increasing cyclohexane content the PMMA blocks collapse and aggregate to form a core to avoid contact with cyclohexane (Scheme 2). For the PS blocks, both ends are connected covalently; one is tethered on the surface, and the other end is connected to the PMMA block. Consequently, their mobility is highly restricted, and we speculate that the PS blocks form a layer around the PMMA core, resulting in an array of surface-immobilized micelles with the domain shape shown in Figure 6. We concluded that this gradual solvent treatment produced samples that displayed a more periodic nanomorphology as deduced by AFM and high water contact angles.

Scheme 2. Speculative Model for Nanopattern from Tethered PS-*b*-PMMA Brushes

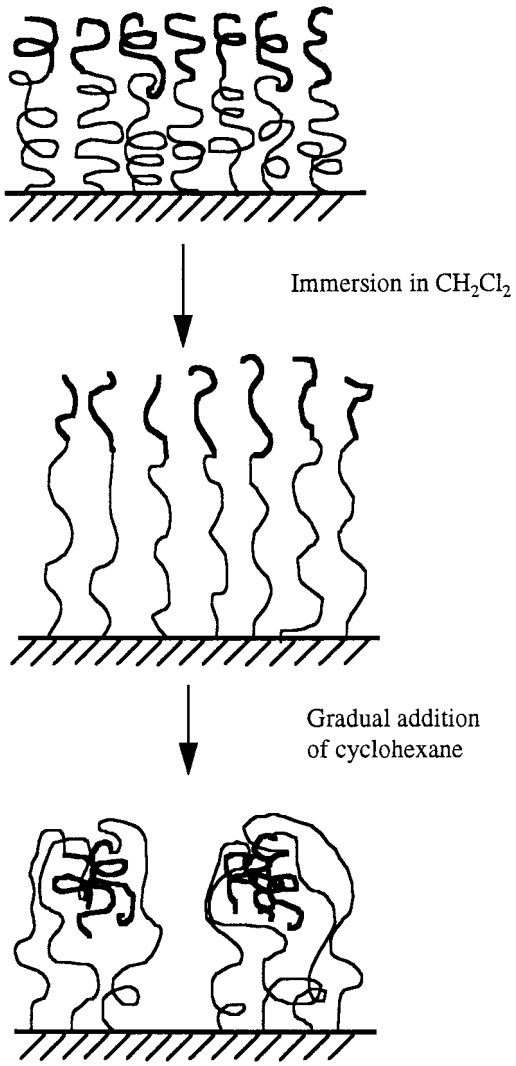

We believe that the average domain size is influenced by the block lengths. We have assumed that the block length is proportional to ellipsometric film thickness. For a tethered PS-*b*-PMMA film with 15 nm PS and 3 nm thick PMMA, the same gradual solvent procedure was applied to this sample. AFM study showed a similar nanomorphology but with different dimensions. The typical diameter of the domain was 46 nm, and the surface roughness of was 5.3 nm. AFM analysis of a PS-*b*-PMMA brush with 26 nm PS and 17 nm PMMA after treatment with the same solvent revealed a similar nanomorphology; the average domain diameter was 113 nm, and the surface roughness was 11.7 nm. Table 1

Table 1. Average AFM Domain Diameter vs Diblock Brush Thickness

PS thickness, nm[a]	PMMA thickness, nm[a]	domain diameter, nm[b]	roughness, nm[b]
15	3	46	5.3
23	14	85	13.1
26	17	113	11.7

[a] Thickness determined by ellipsometry. [b] Domain diameter and roughness determined by AFM.

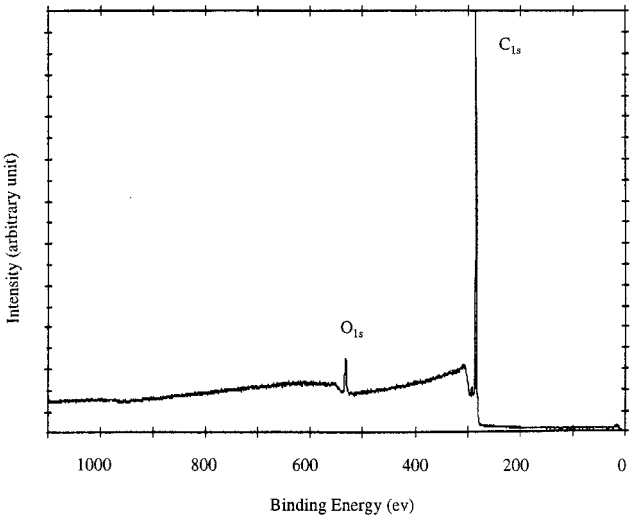

Figure 7. XPS spectrum of the PS-*b*-PMMA brush nanomorphology shown in Figure 6.

contains a summary of the experimental relationship between block lengths (as determined by ellipsometry) vs average domain diameter for the observed nanomorphologies. For the three samples studied, the largest diblock variable is the PMMA thickness. As the thickness of the PMMA layer increases, the average domain diameter of the surface-immobilized micelles also increases. This experimental observation was predicted by Balazs et al.;[2] self-consistent-field theory indicated that pinned micelles should be observed for tethered diblocks where the more soluble block (in our case, PS) is attached to the surface. Furthermore, Balazs and coworkers predicted that the size of the pinned micelles should increase with the size of the less-soluble block (in our case, PMMA), as we have observed.

According to our model for the observed nanomorphology (Scheme 2), the uppermost layer of this structure should be primarily composed of PS. We used XPS analysis (Figure 7) to confirm this prediction. The XPS spectrum for the surface shown in Figure 6 contains a small oxygen peak O_{1s} compared with the C_{1s} carbon peak. Calculations show that the probing region of XPS consisted of 81.7% PS and 18.3% PMMA (mole ratio). Thus, the topmost layer of this surface is primarily composed of PS.

Cyclohexane is a poor solvent for PS. As a control experiment, we studied PS homopolymer brushes with the same mixed solvent of CH_2Cl_2 and cyclohexane where the composition was gradually changed from CH_2Cl_2 to cyclohexane. For a 28 nm thick PS brush, AFM analysis revealed a smooth, featureless surface with a roughness of 0.7 nm. In conclusion, this treatment does not produce a similar nanomorphology as observed for tethered diblock copolymer brushes.

Surface Roughness and Contact Angles. The wettability of a solid surface with a liquid (usually, water) is important in many industrial applications and has been extensively studied from both theoretical and experimental points of view. Contact angles are related to the interfacial free energies through Young's equation,[21]

$$\cos\theta = (\gamma_{sv} - \gamma_{sl})/\gamma_{lv}$$

where θ = the contact angle and γ = interfacial free energy. The values of contact angles are influenced by roughness, chemical composition, morphology, swelling of the solid by the contact liquid, and chemical heterogeneity at the interfacial regions. Surface roughness influences the contact angle values in many ways; important parameters include the roughness length scale and surface topology.[22−25] A common approach to describe the relationship between roughness and contact angles, which was suggested by Wenzel, is shown in the following equation:[26,27]

$$\cos\theta_{obsr} = r\cos\theta_{true}$$

where θ_{obsr} is the observed contact angle, θ_{true} is the true contact angle, and r is a roughness factor, which is defined as the ratio of the actual surface area to the area projected from the surface onto a flat, parallel surface. Besides the effect of surface roughness described by the above equation, a liquid droplet can trap pockets of air to form a "composite" [(solid + air) − liquid] interface, thereby raising the observed contact angles. The contact angle hysteresis which is the difference between the advancing contact angle and receding contact angle has also been studied theoretically and experimentally.[22] Johnson and Dettre proposed that the contact angle hysteresis is explained by a balance between the macroscopic vibrational energy of the liquid droplet and the heights of energy barriers separating metastable states. Hysteresis increases as the energy barrier increases or as the vibrational energy decreases.

According to the Wenzel equation, roughness should increase for contact angles that are greater than 90° and decrease those that are less than 90°.[28,29] Indeed, it was found that the roughening of a smooth nonpolar surface resulted in an increase of advancing contact angle.[23] We have used this equation to explain our experimental observations. For the surface shown in Figure 6, the advancing water contact angle was 120° and the receding contact angle was 94°. From XPS analysis, we have determined that the topmost layer is primarily composed of PS blocks. The characteristic values for PS are 99° and 82°. Roughness did increase the advancing contact angle from 99° to 120° in accord with expectations. However, roughness also increased the receding contact angle from 82° to 94°, which cannot be interpreted by this equation. We do not know at what length scale the surface topological feature is important and at what value the surface roughness increases the values of contact angles.

We observed that a tethered PS-*b*-PMA brush exhibits an advancing contact angle of 68° and a receding contact angle of 55°. A PMA film prepared by spin-casting exhibits advancing and receding contact angles of 83° and 64°. Because the advancing and receding contact angles of PS are larger than 68°, we cannot attribute this result to the presence of PS in the water sensing region. Therefore, we believe that the surface roughness is a likely explanation. As predicted by the Wenzel

equation, surface roughness will decrease contact angles that are less than 90°.

Summary

AFM analysis of tethered PS-*b*-PMMA brushes indicated that various nanomorphologies were formed after treatment with different ratios of CH_2Cl_2 and cyclohexane. If a solvent mixture of CH_2Cl_2 and cyclohexane was used and the composition was gradually changed from CH_2Cl_2 to cyclohexane, an unusual nanomorphology was formed with an advancing water contact angles higher than that of PS. The mechanism of this nanopattern formation was proposed, and the explanation of water contact angles was provided. Compared to PS-*b*-PMMA, PS-*b*-PMA brushes exhibited a different morphology after treatment with CH_2Cl_2. We attributed this difference to the larger Flory−Huggins interaction parameter between PS and PMA vs PS and PMMA. We feel that these tethered diblock copolymer brushes may be useful in surface property control and nanopattern fabrication.

Acknowledgment. This work was financially supported by the Army Research Office (DAAH04-96-1-0018) and The National Science Foundation (DMR-0072977).

References and Notes

(1) Dong, H.; Marko, J. F.; Witten, T. A. *Macromolecules* **1994**, *27*, 6428.
(2) Zhulina, E. B.; Singh, C.; Balazs, A. C. *Macromolecules* **1996**, *29*, 6338.
(3) Zhulina, E. B.; Balazs, A. C. *Macromolecules* **1996**, *29*, 2667.
(4) Zhulina, E. B.; Singh, C.; Balazs, A. C. *Macromolecules* **1996**, *29*, 8254.
(5) Singh, C.; Balazs, A. C. *Macromolecules* **1996**, *29*, 8904.
(6) Balazs, A. C.; Singh, C.; Zhulina, E. B.; Gersappe, D.; Pickett, G. *MRS Bull.* **1997**, *1*, 16.
(7) Gersappe, D.; Fasolka, M.; Israels, R.; Balazs, A. C. *Macromolecules* **1995**, *28*, 4753.
(8) Chern, S.-S.; Zhulina, E. B.; Pickett, G. T.; Balazs, A. C. *J. Chem. Phys.* **1998**, *108*, 5981.
(9) Zhao, B.; Brittain, W. J. *J. Am. Chem. Soc.* **1999**, *121*, 3557.
(10) Zhao, B.; Brittain, W. J. *Macromolecules* **2000**, *33*, 342.
(11) Zhao, B.; Brittain, W. J. *Macromolecules* **2000**, *33*, 8813.
(12) Zhao, B.; Brittain, W. J.; Zhou, W.; Cheng, S. Z. D. *J. Am. Chem. Soc.* **2000**, *122*, 2407.
(13) Tsukruk, V. V. *Rubber Chem. Technol.* **1997**, *70* (3), 430.
(14) Nisato, G.; Ermi, B. D.; Douglas, J. F.; Karim, A. *Macromolecules* **1999**, *32*, 2356.
(15) *Scanning Probe Microscopy of Polymers*; Ratner, B. D., Tsukruk, V. V., Eds.; ACS Symposium Series 694; American Chemical Society: Washington, DC, 1998.
(16) Kelley, T. W.; Schorr, P. A.; Johnson, K. D.; Tirrell, M.; Frisbie, C. D. *Macromolecules* **1998**, *31*, 4297.
(17) Koutsos, V.; Van der Vegte, E. W.; Hadziioannou, G. *Macromolecules* **1999**, *32*, 1233.
(18) Iwata, H.; Hirata, I.; Ikada, Y. *Macromolecules* **1998**, *31*, 3671.
(19) Prucker, O.; Rühe, J. *Langmuir* **1998**, *14*, 6893.
(20) *Physical Properties of Polymers Handbook*; Mark, J. E., Ed.; AIP Press: New York, 1996.
(21) Young, T. *Philos. Trans. R. Soc.* **1905**, *95*, 65.
(22) Johnson, R. E., Jr.; Dettre, R. H. *Adv. Chem. Ser.* **1964**, *43*, 112.
(23) Johnson, R. E., Jr., Dettre, R. H. *Surf. Colloid Sci.* **1969**, *2*, 85.
(24) Andrade, J. D.; Smith, L. M.; Gregonis, D. E. In *Surface and Interfacial Aspects of Biomedical Polymers*; Andrade, J. D., Ed.; Plenum: New York, 1985; Vol. 1, Chapter 7.
(25) Fadeev, D. Y.; McCarthy, T. J. *Langmuir* **1999**, *15*, 3759.
(26) Wenzel, R. N. *J. Phys. Colloid Chem.* **1949**, *53*, 1466.
(27) Ulman, A. *An Introduction to Ultrathin Organic Films*; Academic Press: Boston, 1991.
(28) Good, R. J. *J. Am. Chem. Soc.* **1952**, *74*, 5041.
(29) Eick, J. D.; Good, R. J.; Neumann, A. W. *J. Colloid Interface Sci.* **1975**, *53*, 235.

MA000434E